Study on Wettability Effect on Water Transport in Gas Diffusion Layer of PEFC

by

Enes Muhammet CAN

A thesis submitted in partial fulfillment of the requirements for the degree of Master of Engineering

Examination Committee: Prof. Dr. Tabe YUTAKA
Prof. Dr. Hideyuki OGAWA
Prof. Dr. Tsuyoshi TOTANI

Master's Thesis No. 324
Division of Energy and Environmental Systems
Graduate School of Engineering, Hokkaido University
September 2019

LIST OF ABBREVIATION

IEA	International energy agency
FCs	Fuel Cell Systems
PEFC	Polymer Electrolyte Fuel Cell
HOR	Hydrogen Oxidation Reaction
ORR	Oxygen Reduction Reaction
CCM	Catalyst Coated Membrane
GDL	Gas Diffusion Layer
MEA	Membrane Electrode Assembly
LBM	Lattice Boltzmann Method
MPL	Micro Porous Layer
PTFE	Polytetrafluoroethylene

ABSTRACT

Polymer electrolyte fuel cell (PEFC) systems are one of the most promising technologies which can be used as a power sources of transportation sectors. Its high efficiency and low CO_2 emissions are its biggest advantages over conventional engines. However, under the high current density operations due to the high amount of water production at the cathode side of the PEFC, the diffusion of oxygen to the catalyst layer decreases. This phenomenon results in a strong decrease in fuel cell performance. It is therefore essential to decrease the amount of water inside the gas diffusion layer (GDL), so that the polymer electrolyte fuel cell systems performance can increase. This current study explores the effect of wettability designs with hydrophilic and hydrophobic regions in GDLs to create dedicated pathways for oxygen and water transportation.

The first step in this research was to observe water behavior inside of the GDL, through the Lattice Boltzmann Method simulation and scale model experiment. Furthermore, hydrophilic surface treatment with 85°C contact angle is applied on hydrophobic GDL, and is analyzed by LBM simulation and scale model experiment. Experimental results show that the extremely high amount of water in the GDL, mainly caused by water accumulation under the rib, has decreased successfully through hydrophilic surface treatment.

In the second part of this research, three different designs have been applied on the GDL. These designs are a) dot design, b) 2mm-2mm stripped design and c) 2mm-6mm stripped design. In order to create hydrophobic patterns, the GDL is coated with polytetrafluoroethylene (PTFE), respectively with ten, twenty, and sixty percent solutions. Moreover, the newly designed GDLs have been tested in a single fuel cell test station and its performance has been evaluated by I-V curves. Results shows that a 2mm-2mm striped design with ten percent PTFE coating gives the best results, as it enables a high interaction area between hydrophilic and hydrophobic regions.

Keywords: polymer electrolyte fuel cells, gas diffusion layer, wettability, Lattice Boltzmann method, scale model experiment.

TABLE OF CONTENTS

1. INTRODUCTION

1.1 Introduction

According to the International Energy Agency (IEA) in 2016, our global electricity production increased by 2.9 per cent [1]. The report of IEA states that 67.3 per cent of electricity derives from combustible fuels, which highly correlates with carbon dioxide (CO_2) emissions. Figure 1.1 shows the share of fossil fuels in electricity production by countries in 2016 [Figure 1.1]. In the same report it is mentioned that the share of renewable energy resources for the production of electricity was just 5.6 per cent in the same year.

Although our energy consumption is ever increasing, the availability of fossil fuel sources is near diminishing. Forecasts show that our fossil fuels will not last more than 100 years [2]. Moreover, with the increasing CO_2 emissions, global warming threatens life across the globe in equal but destroying ways. Unfortunately, our primary energy sources are concentrated at politically and economically unstable countries, mostly of them in Third World countries. For countries that do not have sufficient energy resources available on own grounds, a phenomenon referred to as self-sufficiency, this is an issue. Figure 1.2 shows the statistic of self-sufficiency in 2016.

Promising but still fairly far from its true potential, renewable energy is the most prominent solution to the above-described issues, by diminishing our needs for fossil fuels.

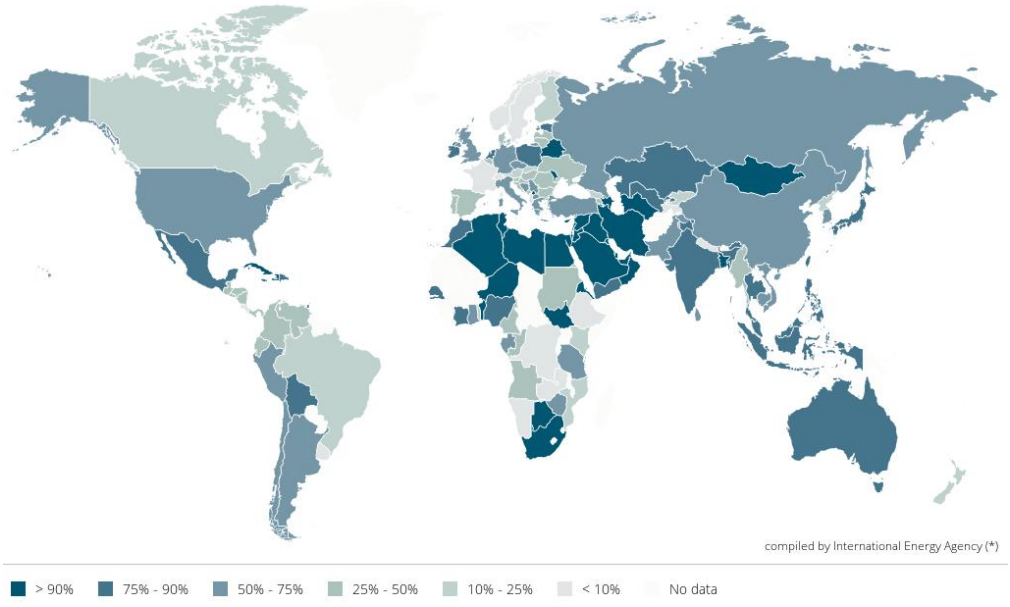

Figure 1.1 Share of fossil fuels in electricity production by countries (2016) [1]

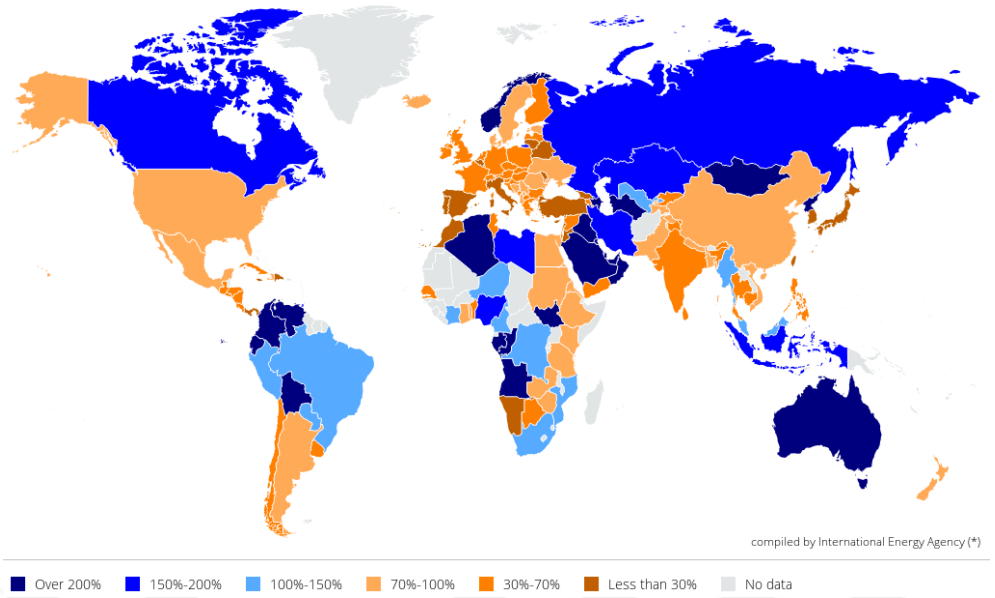

Figure 1.2 Self-sufficiency of the countries in terms of fossil fuels production (2016) [1]

However, these new technologies have many challenges. A very simple but actual example are the photovoltaic panels and wind turbines, which need large areas to produce enough electricity. In addition, they are highly affected by weather conditions and have very specific requirements regarding their geographical location and build. Moreover, these are not suitable energy sources for vehicles. As vehicles are the largest in consuming fossil energy, this category is in need of a solution on its own.

In this regard fuel cell systems (FCs) and the associated hydrogen related technologies can be a better choice to overcome the energy crisis that we are facing in our current society. In addition, hydrogen is one of the most reliable secondary energy that will contribute to reduce greenhouse gasses and energy security. Most importantly, hydrogen can be produced from numerous energy sources without discharging CO_2. Polymer electrolyte fuel cell (PEFC) systems are regarded as the most promising renewable energy technologies for transportation. Coming with higher costs, however, the biggest challenge for its commercialization. In order to spread its utilization in society and make it commercially available, cost reduction is a crucial factor in the development of PEFCs.

1.2 Relevance and Objectives

After oxygen reduction reaction (ORR) at and hydrogen oxidation reaction (HOR) in PEFCs at the cathode side, water is produced as a product. However, under the high current density operations, due to the excessive water accumulation inside of the GDL, the oxygen diffusivity decreases dramatically. This phenomenon results in sharp performance decrease in the system.

Pasaogullari and Wang [3] studied the physic behind the water transport in both hydrophilic and hydrophobic diffusion media and found that liquid water transport in the GDL is controlled by capillary forces. In addition, many other recent studies [9] show that increasing in hydrophobicity of the GDL with polytetrafluoroethylene (PTFE) coating improves water management inside of the structure. However, after a certain amount, PTFE particles accumulate in certain location inside of the GDL: this start to block pores of GDL and result in water accumulation in it. Also, it is known that water tend to accumulate in the hydrophilic structure and hydrophobic structure is more flooding tolerant. Thus, it is important to create dedicated pathways for water which cannot block oxygen transport to the catalyst layer.

Objective of this study is creating dedicated path ways with hydrophobic and hydrophilic regions to increase oxygen diffusivity to the catalyst layer,

This research examines the hydrophobic regions in hydrophilic GDL and hydrophilic regions in hydrophobic GDL with different pattern designs to increase fuel cell performance. Hydrophilic surface treatment on GDL, which has analyzed by Lattice Boltzmann method (LBM) and 240 times enlarged GDL model, will also be further researched.

1.3 Fuel Cells

Fuel cells are simple electrochemical devises which convert the chemical energy of hydrogen into electricity. In these systems hydrogen is used as a fuel and after it interact with oxygen, energy is released. This process might be perceived as burning fuel directly but is very different if further examined. In the fuel cells, hydrogen and oxygen molecules interact and form water. The energy of in the bounding configuration of water is lower than that of hydrogen and oxygen molecules before the reaction. These energy differences are produced as an electricity in fuel cells. On the other hand, conventional engines, the first heat is produced after burning fuel and heat is converted to mechanical work then electricity. In this conversion processes are inefficient. This means that fuel cells are more efficient than combustion engines. Because in a fuel cell electricity is directly obtained from the occurring electrochemical reaction.

In order to transfer electrons through a certain path, hydrogen and oxygen reactions are spatially separated by an electrolyte in the fuel cell. In this way liberated electrons from hydrogen oxidation reaction cannot penetrate through electrolyte to oxidation reduction reaction sides. In this way, the resulting energy can easily be harnessed.

1.4 Different Types of Fuel Cells

Fuel cells are classified depending on the electrolyte type which it employs. There are five major fuel cells types; (1) phosphoric acid fuel cells, (2) polymer electrolyte membrane fuel cells, (3) alkaline fuel cells; (4) molten carbonate fuel cells; (5) solid-oxide fuel cells.

Even though these different type of fuel cells have different electrolytes, different materials and operation temperatures, the underlying electrochemical principle is similar. Their performance characteristics are also different. A comparison between these fuel cells are given in Table 1.

Table 1. Comparison of various types of fuel cell

	PEMFC	PAFC	AFC	MCFC	SOFC
Electrolyte	Proton Exchange Membrane (PEM)	Liquid H_3PO_4	Liquid KOH	Molten carbonate	Ceramic
Charge carrier ion	H^+	H^+	OH^-	CO_3^{-2}	O^{-2}
Operating Temperature	60-80 °C	200 °C	60-220 °C	650 °C	600-1000 °C
Reaction Catalyst	Platinum	Platinum	Platinum	Nickel	Perovskites
Cell Components	Carbon Based	Carbon Based	Carbon Based	Steel Based	Ceramic Based
Fuel	H_2, Methanol	H_2	H_2	H_2, CH_4	H_2, CH_4, CO

1.5 Polymer Electrolyte Fuel Cells

In PEFC systems, electrolyte sulfonated tetrafluoroethylene (Nafion, a patented material of Dupont) are employed. Nafion membrane blocks movement of electrons and allows protons pass through. PEFCs are preferred mainly for transportation due to the low operational temperature and high-power density.

The electrochemical half-cell reaction in a hydrogen fueled PEMFC is as follows.

$$H_2 \rightarrow 2H^+ + 2e^-$$

$$O_2 + 4H^+ + 2e^- \rightarrow 2H_2O$$

As can be seen, there are two half-cell reactions occurring inside the system. At the anode side there is hydrogen oxidation reaction (HOR) and at the cathode side oxygen reduction reaction (ORR). As a result of HOR electrons are liberated and they follow a certain path to combine with oxygens and protons at the anode side. After this phenomena water is produced at the ORR side.

HOR and ORR reactions take place at the surface of a platinum catalyst. Figure 1.3 shows a schematic diagram of a typical PEFC.

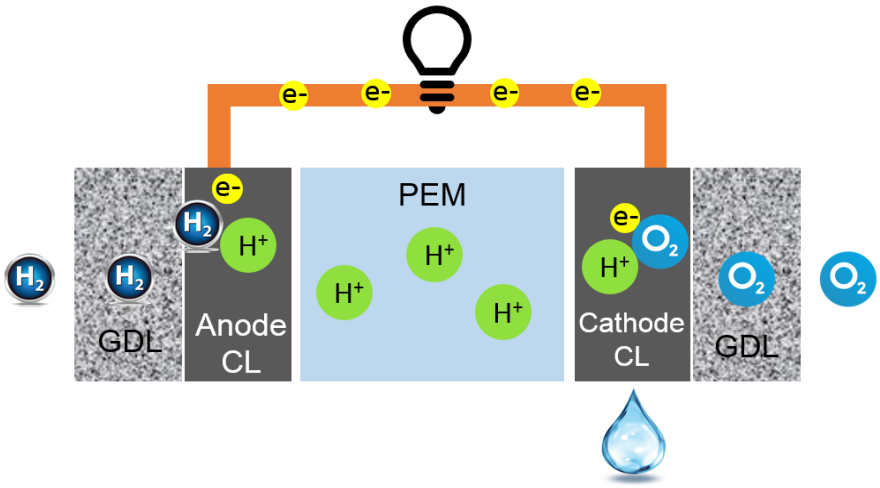

Figure 1.3 Schematic diagram of a typical hydrogen PEFC

A single cell contains two gas diffusion layers (GDL) for each reaction side and a catalyst coated membrane is sandwiched between two GDLs. Catalyst coated membrane (CCM) is the heart of the system which contains two catalyst layers. These two catalyst layers are separated by a membrane. Usually platinum nano particles are supported on carbon in the catalyst layer. GDL is used in the system to increase the diffusivity of fuel gases and to mechanically support to CCM. GDL and CCM assembly is collectively called the membrane electrode assembly (MEA).

On the outer side, a member for supplying fuel called a separator is incorporated. Hydrogen gas supplied at the anode side is oxidized at the anode electrode and separated into protons and electrons. The separated electrons move to the cathode via an external circuit. Proton moves to the cathode via the electrolyte membrane. Then, it reacts with the oxygen supplied to the cathode electrode to become water. It is the movement of electrons in the external path that corresponds to the current.

The produced current by a fuel cell increases with the size of the reaction area. Reaction area is the active area where electrolyte, and the electrodes meet. In order to increase the produced current or in other saying electricity it is necessary to increase reaction area. To make larger reaction surfaces, fuel cells are usually made into thin, planar structures. (Figure 1.4) In addition, to enlarge the reaction surface area, electrodes are made highly porous allowing larger flows

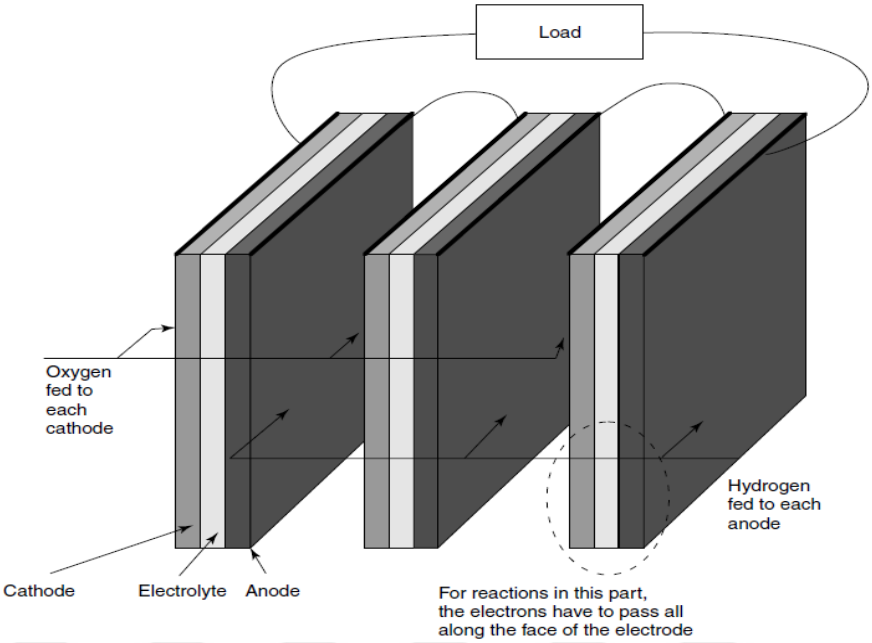

Figure 1.4 Series arrangement of typical hydrogen PEMFC [4]

There are five important steps to design a fuel cell. These steps are as follows: (1) reactant delivery (transport) into the fuel cells: (2) electrochemical reaction; (3) proton conduction through the electrolytes; (4) electronic conduction through the external circuit; (5) product removal from the fuel cells.

1.6 Fuel Cell Performance Characteristics

The performance of fuel cells generally sums up with current-voltage characteristics called polarization curves or simply the I-V curves. As mentioned in the previous section, depending on the reaction area, produced current (electricity) is increased. Hence, to compare the performance of different cells which has different reaction area is possible after current is normalized by the cell area. I-V curves enable comparison between cells of different area.

In theory an ideal fuel cell can supply desired current while maintaining a constant current. Thermodynamically determined voltage is 1.23V. However, in actual operational conditions the voltage is lower than the thermodynamically determined voltage. Likewise, with increase in current density voltage further drops. This limits the total power output. Power

density curve can be obtained from I-V curve by multiplying current density and corresponding voltage. Figure 1.5 is an example of current density and power density curves.

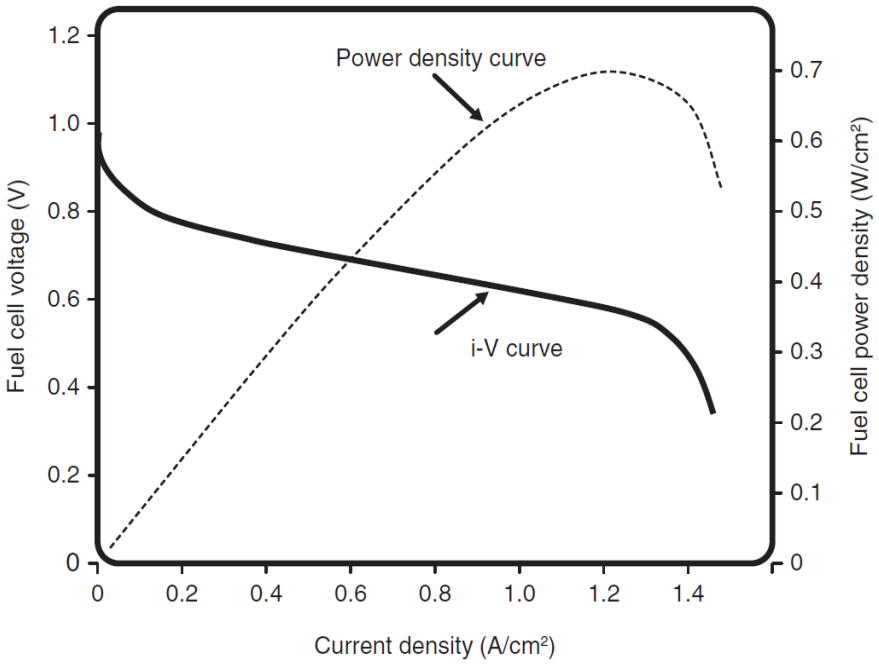

Figure 1.5 Combined I-V and power density curve of typical hydrogen PEMFC [4]

Until it reaches its maximum, power density of a fuel cell increases in current density. Then, after hitting it maximum power density decreases with increase in current density Usually, this peak of power density forms the limit of fuel cell operations. Beyond this point, even though current density is increased, due to the sharp drop in the cell, voltage will cause a significant drop in power density.

Hydrogen consumption in a PEFC is proportional to the current density. In addition, decrease in fuel cell voltage causes decrease in power density. In this regard, voltage axis can be considered as the efficiency axis of a fuel cell.

Desirable condition in order to spread the usage of fuel cell systems, is maintaining high voltage under the high current density operation. However, it is hard to maintain a high fuel cell voltage under the high current load. This is due to the irreversible losses in the cell. Furthermore, the more current that is drawn from full cell, the greater are these losses. Losses in the fuel cell can be classified in three major categories, which give a fuel cell its characteristic shape: (1) activation losses (losses due to electrochemical reaction); (2) ohmic losses (losses due to ionic and electronic conduction); (3) concentration losses (losses due to mass transport).

As shown in Figure 1.6, the I-V curve can be divided to 3 part. The first part encompasses the activation regions, the ohmic region is the middle section of the curve and last part is the mass transport region. The losses in these three regions will be explained next subsections.

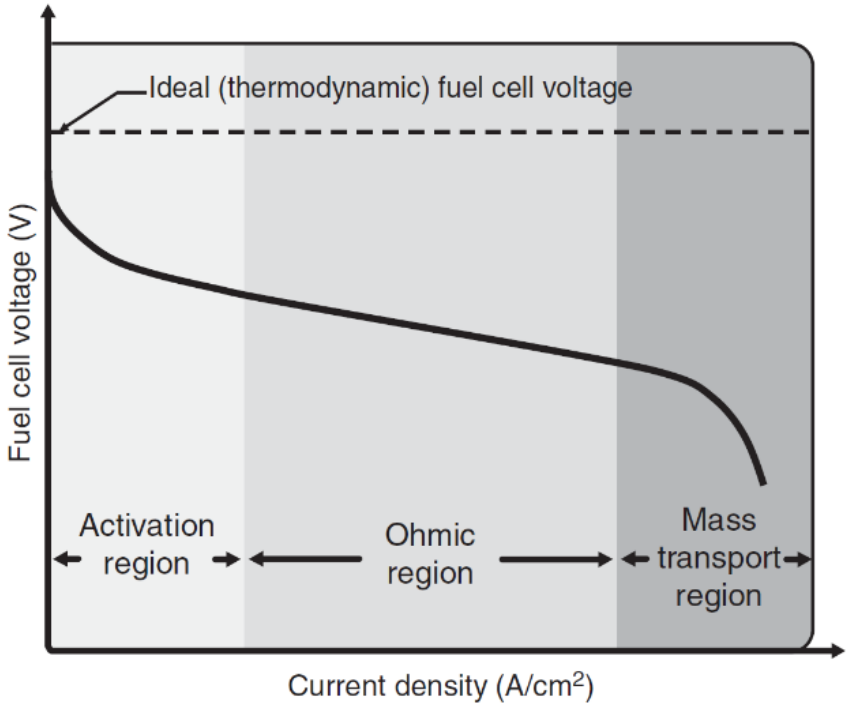

Figure 1.6 Major losses that contribute to the characteristic shape of the fuel cell I-V curve [4]

1.6.1 Activation Losses

This loss is mainly because of the reaction speed which is occurring on the surface of the electrodes. A part of the generated voltage is utilized to transfer electrons from or to the electrode. These reaction losses arise during the start of the reaction and more dominant at low current densities (<100 mA/cm^2).

1.6.2 Ohmic Losses

Ohmic losses are generally occurring due to the resistance to the flow of electrons through the material of the electrodes, interconnection of the cell and to resistance of electrolyte against flow of ions. These losses can be observed intermediate current densities. This voltage decreases especially proportional to the current density.

1.6.3 Concentration Losses

These losses are also called mass transport losses. They are mainly due to the decrease in concertation of reactants. These losses are predominant at the high current densities which are generally more than 500 mA/cm^2. Especially in PEFCs, due to the excessive water production at the cathode side due to the ORR reaction, the diffusivity of oxygen decreases dramatically. In order to decrease concentration losses, it is crucial to improve GDL performance. In the present study author introduces a wettability design for GDL which improve its performance.

1.7 Fuel Cell Efficiency

One of the biggest advantages of implementing fuel cells in the internal combustion engines is its efficiency. Despite the assumptions that fuel cells are fully efficient, this is not true in practice. Even in there would be an ideal fuel cell, the extracted electrical work is limited by Gibbs free energy. In case of real fuel cells, efficiency is much less due to the irreversible losses during operation.

The efficiency of a conversion system can be express by following formula.

$$\text{Efficiency } (\eta) = \frac{\text{usefull energy}}{\text{total energy}}$$

Here, useful energy can be defined as the amount of energy can be produce from a system. In addition, the efficiency of a heat engine can be calculated by following formula.

$$\text{Efficiency } (\eta) = \frac{\text{Tmax} - \text{Tmin}}{\text{Tmax}}$$

If we address the efficiency of a fuel cell, it will be as below.

$$\text{Efficiency } (\eta) = \frac{\Delta \text{G}}{\Delta \text{H}}$$

Here ΔG is Gibbs free energy and ΔH is higher heating value of the fuel cell reaction. Also,

$$\Delta \text{G} = \Delta \text{H} - \text{T}\Delta \text{S}$$

$$\text{Efficiency } (\eta) = 1 - \frac{T\Delta S}{\Delta H}$$

As it seen from above formulation, efficiency decreases as temperature increases. Thus, fuel cells have higher efficiency for ambient conditions. While the efficiency of a heat engine is around 50 per cent depending upon the operating temperature, theoretical efficiency of a fuel cell is around 83 per cent. Figure 1.7 gives a comparison between efficiencies of fuel cell and heat engine.

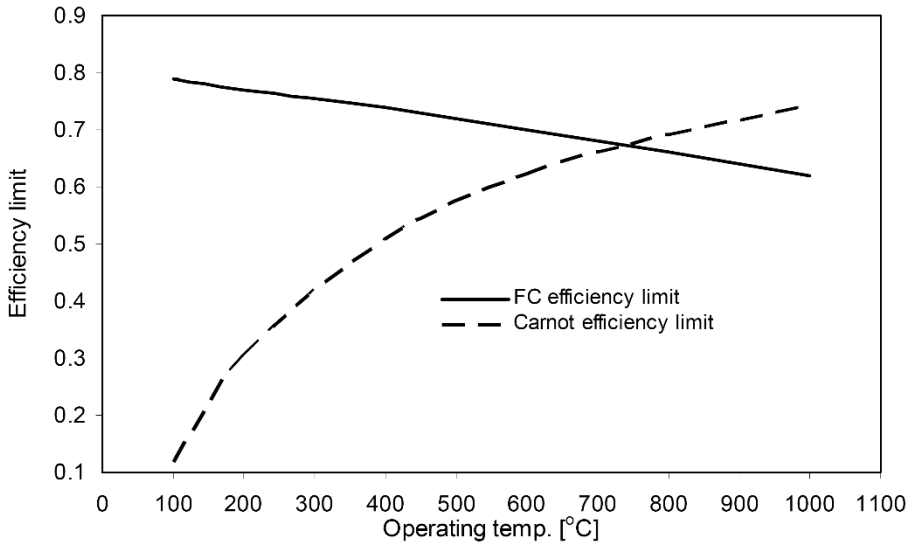

Figure 1.7 Comparison between efficiencies of fuel cell and heat engine [4]

1.8 Contact Angle and Wetting Properties

A contact angle is the angle between a solid surface and a liquid drop which placed on it in another immiscible fluids. A contact angle is a very convenient way to measure the wettability of a material. The contact angle of a liquid drop on a material is determined by the mechanical equilibrium under the there interfacial tensions.

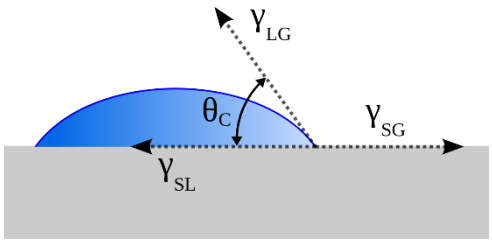

Figure 1.8 Illustration of action of three interfacial tensions on a droplet

The mechanical equilibrium which firstly described by Thomas Young is;

$$\gamma sg - \gamma sl - \gamma \lg * cos\theta c = 0$$

Whereas γsg, γsl and γlg represent solid-vapor, solid-liquid and liquid-vapor interfacial tensions respectively, θc is Young's contact angle. Furhermore, if the contact angle is less than 90° it is called the hydrophilic surface. If the hydrophilic surface is greater than 90°, it is called hydrophobic surface.

In terms of hydrophilic and hydophobic GDL cases, water tends to accumulate inside of the hydrophilic GDL more than hydrophobic GDL due to the capillary pressure [3].

2. EXPERIMENTAL SETUP

In this research three different kind of experimental methods have been conducted. To observe water behavior in GDL with hydrophilic surface treatment, a scale model experiment and Lattice Boltzmann Method (LBM) simulation have been conducted. In addition, to evaluate different wettability designs a single cell experiment has been conducted. As a preparation of the single cell experiment, catalyst coated membrane (CCM) was fabricated and GDLs with different wettability patterned were produced.

In this section the single cell experimental setup, CCM fabrication and GDLs coating are explained. The details of the scale model experiment and LBM simulation are explained in the next chapter.

2.1 Single Fuel Cell Test Equipment

Single cell with a 25 cm^2 active area was fabricated with separators, end plates and gaskets. Figure 2.1 shows the components of the single fuel cell used for this experiment. Polymer electrolyte membrane (Nafion) is sandwiched between cathode and anode catalyst layers, and CCMs are fabricated in the laboratory. For anode side, GDL having a micro porous layer (MPL) was employed from SGL Carbon (Sigracet® GDL 28 BC) [5]. For the cathode side of, GDL from SGL carbon (Sigracet® GDL 39 AA) [5] without MPL coating has been employed. The above mentioned two GDL attached to both sides of the CCM to make MEA. Separator is designed to supply gases to the catalyst layer with provision to place probes for current collection and measurements. Further, to measure the temperature of the cell, a hole for inserting a thermocouple is provided in the separator on the anode side. Membrane electrode assembly is placed between the anode and cathode separators with gaskets and cell is assembled using fasteners at specified torque.

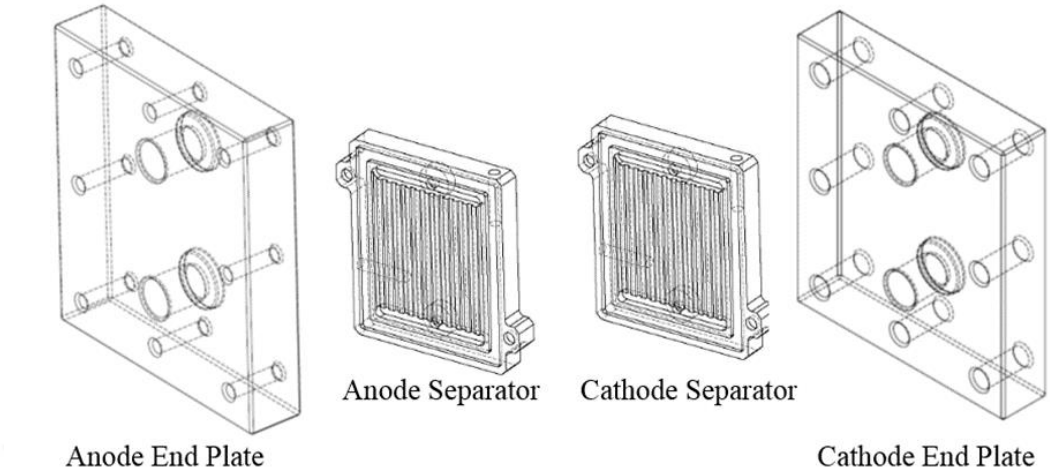

Figure 2.1 Components of the single fuel cell

Figure 2.2 shows the image of single fuel cell used for this research. Important parameters of this single fuel cell are given in Table 2.1.

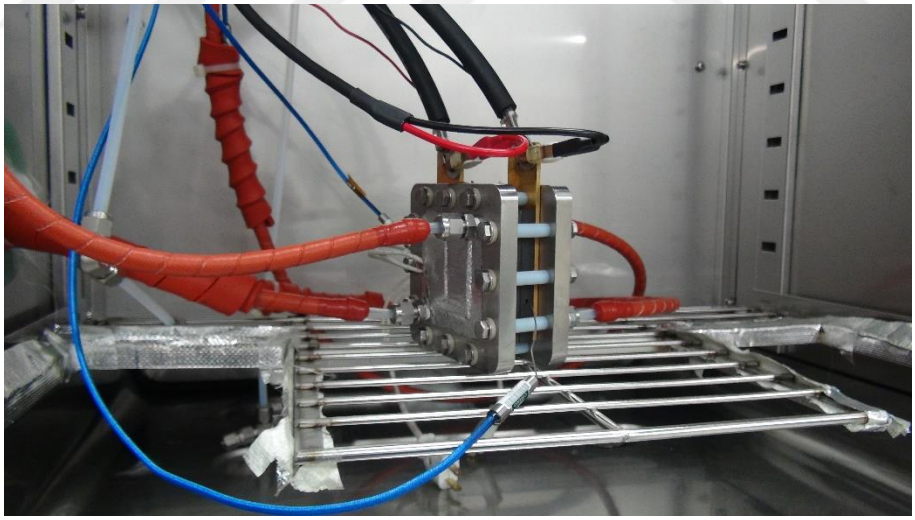

Figure 2.2 Single fuel cell used for this research

Table 2.1 Parameters of the anode and cathode separators

Parameter	Anode	Cathode
Rib width	0.5 mm	0.5 mm
Channel width	0.5 mm	0.5 mm
Channel height	0.3 mm	0.3 mm
Active area dimensions	50 mm X 50 mm	50 mm X 50 mm
Number of channels	50	50

2.2 Fuel Cell Test Station

Test station which is used in this research is shown in Figure 2.3. As a test load electronic load (Kikusui PLZ164WA) was employed and used to record data for I-V curves. This load is used to provide desired resistive load on the fuel cell. Our test station has the ability to precisely control cell temperature, humidity and gas flows. Temperature in pipes and humidifier is closely monitored on the display. For cell temperature control the unit was places in benchtop type temperature chamber Espec SU-241. Figure 2.4 shows the schematic diagram of the test station.

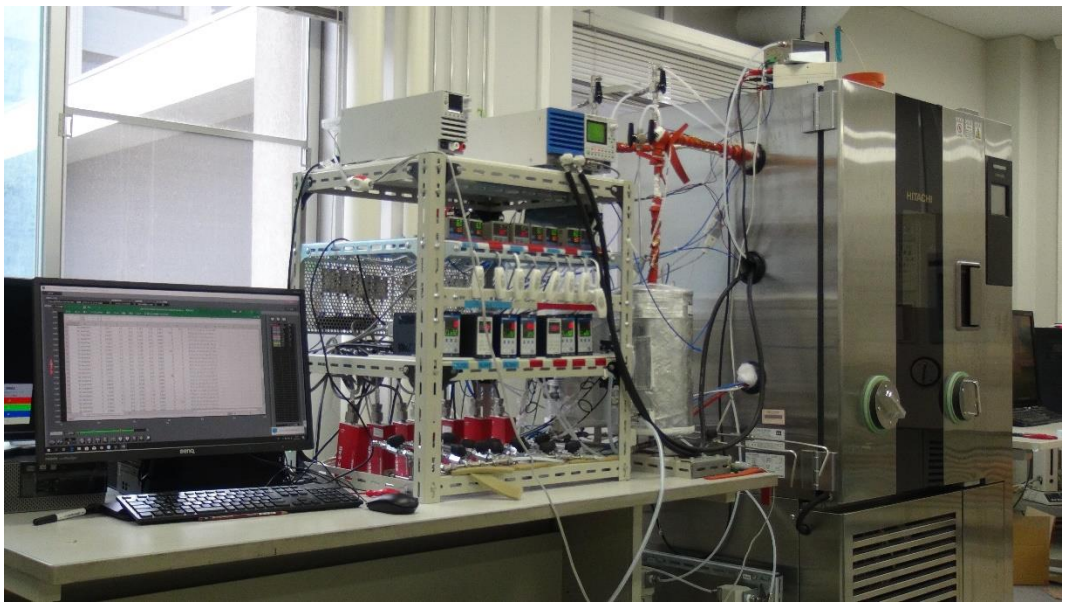

Figure 2.3 Test Station

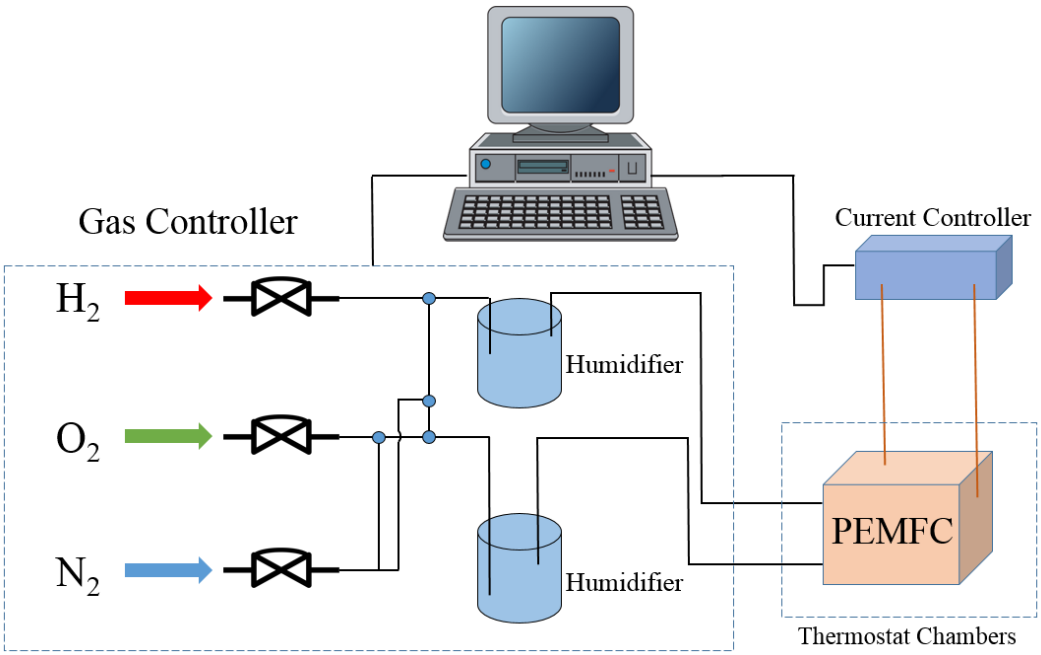

Figure 2.4 Schematic diagram of test station

Table 2.2 shows the typical settings of various parameters for a normal experiment. In this experiment as cathode gas 21 per cent oxygen and 79 per cent nitrogen have been used. For all experiments relative humidity has been kept about 90 per cent. Before testing the samples, the cell dry purged for fifteen minutes and wet purged for five minutes in order to attain stability before taking measurement for experiment.

Table 2.2 Experimental setting parameters

Parameter	Value
Cell temperature	42 °C
Anode gas flow	0.5 L/min
Cathode gas flow	0.5 L/min
Anode humidifier temperature	40 °C

Anode plumbing temperature	40 °C
Cathode humidifier temperature	40 °C
Cathode plumbing temperature	40 °C

2.3 Preparation of Catalyst Coated Membrane

In this research, employed CCM and MEA has prepared in the laboratory.

2.3.1 Preparation of Catalyst Ink

Catalyst ink was prepared by mixing platinum supported on carbon from Tanaka Kikinzoku with Nafion 5 per cent perfluorinated resin solution from Dupont, 2- propanol from Fujifilm Wako and water. In order to prevent from oxidation of platinum, 0.5 g of C/Pt firstly mixed with 1.63 g distilled H_2O in a 100 ml hermetic cup by shaking it slowly by hand for 30 second. After this process 1.63 g 2- propanol, 4.3 g Nafion and 9 g Zr beads has added. The catalyst ink mixture (Figure 2.5) has been putted in the ball mill mixer (NBK-1 Non-Bubbling Kneader) (Figure 2.6) for one hour at 350 rpm. All chemicals were weighted by a balance (A&D GR-202) (Figure 2.6). In this way the amount of Pt loading was optimized between 0.20-0.26 mg/cm^2.

Figure 2.5 Catalyst ink mixture

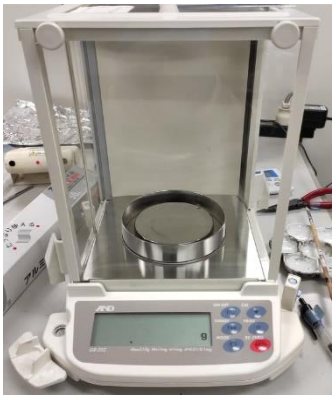

Figure 2.6 On the left the balance and on the right the ball mill mixer

2.3.2 Fabrication of CCM from Catalyst Ink

The catalyst ink is placed on a Teflon sheet which has 150µm thickness using the doctor blade film applicator (Auto film applicator from Tester Sangyo) (Figure 2.7 (a), (b), (c)). The thickness of wet coating is 130µm. After coating catalyst ink on the Teflon sheet, it was placed in an oven for fifteen minutes at 60°C to dry out. After cutting the Teflon sheet in desired size, it is placed on the both side of the polymer electrolyte membrane and hot pressed using hydraulic press at 150°C for ten minutes at 20 MPa pressure (Figure 2.7 (d)). The Teflon sheet from both sides were just conveniently peeled off leaving behind a catalyst coated membrane (Figure 2.7 (e)). Cathode and anode electrodes have been weighted by a balance (A&D GR-202) before and after hydraulic pressing in order to calculate platinum loading in CCM. All platinum loading in this research is around 20 weight per cent. The CCM prepared by this method was mounted on the single fuel cell by sandwiching between gas diffusion layers (GDL) on both sides and tested on fuel cell test load (Figure 2.7 (f)).

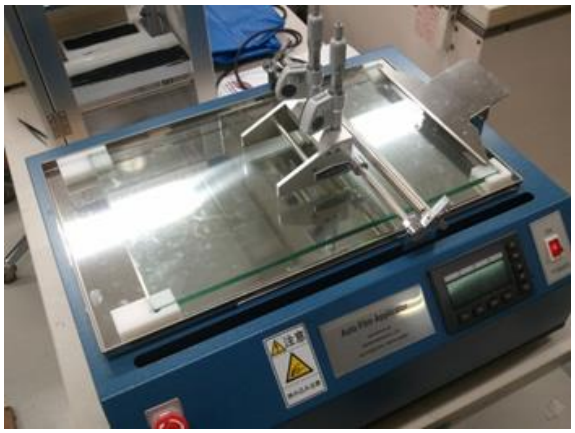

(a)

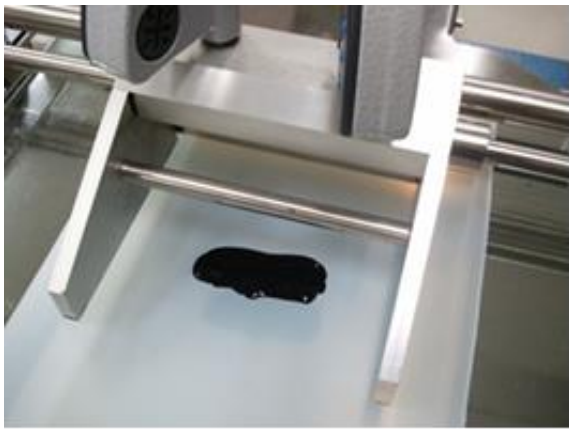

(b)

(c)

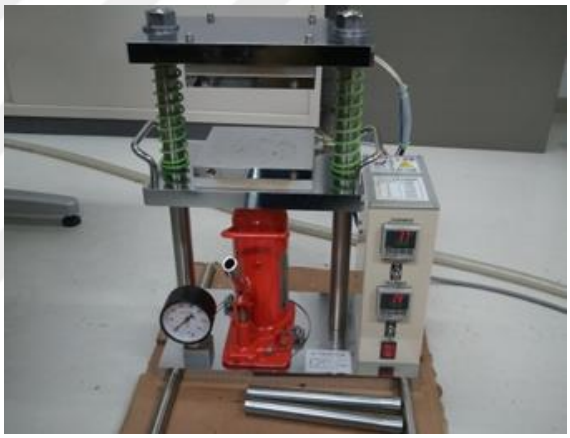

(d)

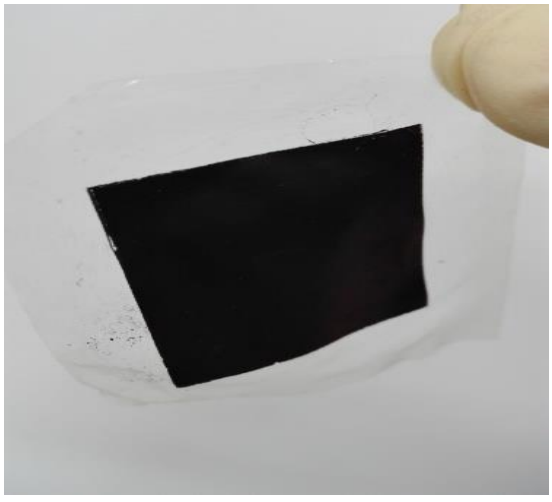

(e)

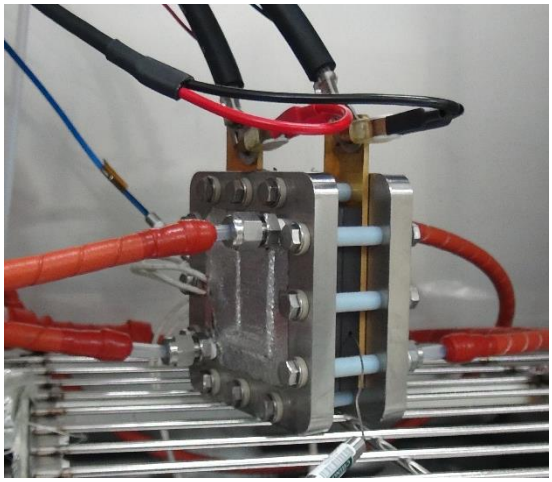

(f)

Figure 2.7 Process of fabrication catalyst coated membrane (CCM)

3. LBM SIMULATION AND SCALE MODEL EXPERIMENT

3.1 LBM Simulation

The Lattice Boltzmann Method (LBM) is very easy to apply to the complex boundary due to the simplicity of its algorithm. Applying parallel computing is also very easy in this method. This makes the LBM a very suitable simulation model to simulate flow behavior inside complex structures, such as in a GDL.

The LBM is a simulation method which analyzes fluid movement in a structure by tracking of particle ensembles. Distribution functions have been used to express the particle density. The time evolution of the distribution function is calculated by a simple law of collision and transition. In addition, in order to simulate multi-phase flow, the interaction of the particles is introduced in the equation. To increase the computational speed of large-scale three-dimensional simulations in the complex GDL structure, the LBM for two-phase flow with the same densities, considering the effect of wettability, was developed previously by our group [6]. They precisely simulated water motion in a large-scale simulation which include a GDL and a channel to show the maximum limit of the Capillary number which maintains similar flow patterns. In the simulation model, the non-dimensional variables are defined by a characteristic length L, a characteristic particle speed c, and a characteristic time scale $t_0 = L/U$, where U is a characteristic flow speed [7]. For velocities of the particle ensembles the three-dimensional 15 velocities model has been used. In this model velocities of particles are restricted to the $\hat{\boldsymbol{c}}_i$ (i = 1, 2,...,15) vectors [6]. The $\hat{f}_i$ and $\hat{g}_i$, are used as two particle velocity distribution functions. In order to distinguish the gas and liquid phases the order parameter $\hat{\phi}$ has been calculated via $\hat{f}_i$ function. $\hat{\phi} < \hat{\phi}_G$, $\hat{\phi} > \hat{\phi}_L$ correspond to the gas and liquid phases, respectively. Also $\hat{\phi}_G \le \hat{\phi} \le \hat{\phi}_L$ is the condition at the interface between the liquid and gas phases. To calculate the velocity of the two-phase flow, $\hat{g}_i$ function is used. The time evolutions of $\hat{f}_i$ and $\hat{g}_i$ with particle ensemble velocity $\hat{\boldsymbol{c}}_i$ at point $\hat{\boldsymbol{x}}$ at a time $\hat{t}$ are computed by the following equations

$$\hat{f}_i(\hat{\mathbf{x}}+\hat{\mathbf{c}}_i\Delta\hat{t},\hat{t}+\Delta\hat{t}) = \hat{f}_i(\hat{\mathbf{x}},\hat{t}) - \frac{1}{\tau_f}[\hat{f}_i(\hat{\mathbf{x}},\hat{t}) - \hat{f}_i^{eq}(\hat{\mathbf{x}},\hat{t})] \tag{1}$$

$$\hat{g}_i(\hat{\mathbf{x}}+\hat{\mathbf{c}}_i\Delta\hat{t},\hat{t}+\Delta\hat{t}) = \hat{g}_i(\hat{\mathbf{x}},\hat{t}) - \frac{1}{\tau_g}[\hat{g}_i(\hat{\mathbf{x}},\hat{t}) - \hat{g}_i^{eq}(\hat{\mathbf{x}},\hat{t})] \tag{2}$$

Here, $\hat{f}_i^{eq}$ and $\hat{g}_i^{eq}$ are the equilibrium distribution functions, and τ_f and τ_g are dimensionless relaxation times. The $\Delta\hat{t}$ is the time step and given by $\Delta\hat{t} = \Delta\hat{x}/\hat{c}$, where $\Delta\hat{x}$ is the spacing of the cubic lattice points. The order parameter $\hat{\phi}$ distinguishing two phases and the velocity of a two-phase fluid $\hat{\mathbf{u}}$ are obtained from the following equations using $\hat{f}_i$ and $\hat{g}_i$.

$$\hat{\phi} = \sum_{i=1}^{15} \hat{f}_i \tag{3}$$

$$\hat{\mathbf{u}} = \sum_{i=1}^{15} \hat{\mathbf{c}}_i \hat{g}_i \tag{4}$$

The local equilibrium distribution functions $\hat{f}_i^{eq}$ and $\hat{g}_i^{eq}$ in Eqs. (1) and (2) are given by the following equations,

$$\hat{f}_i^{eq} = H_i\hat{\phi} + F_i\left[\hat{p}_0 - \kappa_f\hat{\phi}\frac{\partial^2\hat{\phi}}{\partial\hat{x}_\alpha^2} - \frac{\kappa_f}{6}\left(\frac{\partial\hat{\phi}}{\partial\hat{x}_\alpha}\right)^2\right] + 3E_i\hat{\phi}\hat{c}_{i\alpha}\hat{u}_\alpha + E_i\kappa_f G_{\alpha\beta}(\hat{\phi})\hat{c}_{i\alpha}\hat{c}_{i\beta} \tag{5}$$

$$\hat{g}_i^{eq} = E_i\left[3\hat{p} + 3\hat{c}_{i\alpha}\hat{u}_\alpha - \frac{3}{2}\hat{u}_\alpha\hat{u}_\alpha + \frac{9}{2}\hat{c}_{i\alpha}\hat{c}_{i\beta}\hat{u}_\alpha\hat{u}_\beta + A\Delta\hat{x}\left(\frac{\partial\hat{u}_\beta}{\partial\hat{x}_\alpha} + \frac{\partial\hat{u}_\alpha}{\partial\hat{x}_\beta}\right)\hat{c}_{i\alpha}\hat{c}_{i\beta}\right] + E_i\kappa_g G_{\alpha\beta}(\hat{\phi})\hat{c}_{i\alpha}\hat{c}_{i\beta} \tag{6}$$

where α, β, and γ represent the Cartesian coordinates following the summation convention. In the above equations, κ_f is a constant parameter determining the width of the interface between two phases, and κ_g is a constant parameter determining the strength of the surface tension. The other parameters are detailed in reference [6].

$$\hat{\sigma} = \kappa_g\int_{-\infty}^{\infty}\left(\frac{\partial\hat{\phi}}{\partial\hat{\xi}}\right)^2 d\hat{\xi} \tag{7}$$

$$\hat{\mu} = \frac{1}{3}\left(\tau_g - \frac{1}{2} - \frac{2}{3}A\right)\Delta\hat{x} \tag{8}$$

$$\hat{p} = \frac{1}{3}\sum_{i=1}^{15}\hat{g}_i \tag{9}$$

Here, $\hat{\xi}$ is the coordinate perpendicular to the interface, and A is a constant parameter related to the fluid viscosity. The effect of wettability is introduced by assuming the order parameter $\hat{\phi}$ of the solid wall. Since the intermolecular force is expressed in terms of the order parameter of the fluid in the LBM, giving the order parameter of the solid wall corresponds to giving the intermolecular force between liquid and the solid wall. Figure 3.1 shows visualization of simulation domain and boundaries.

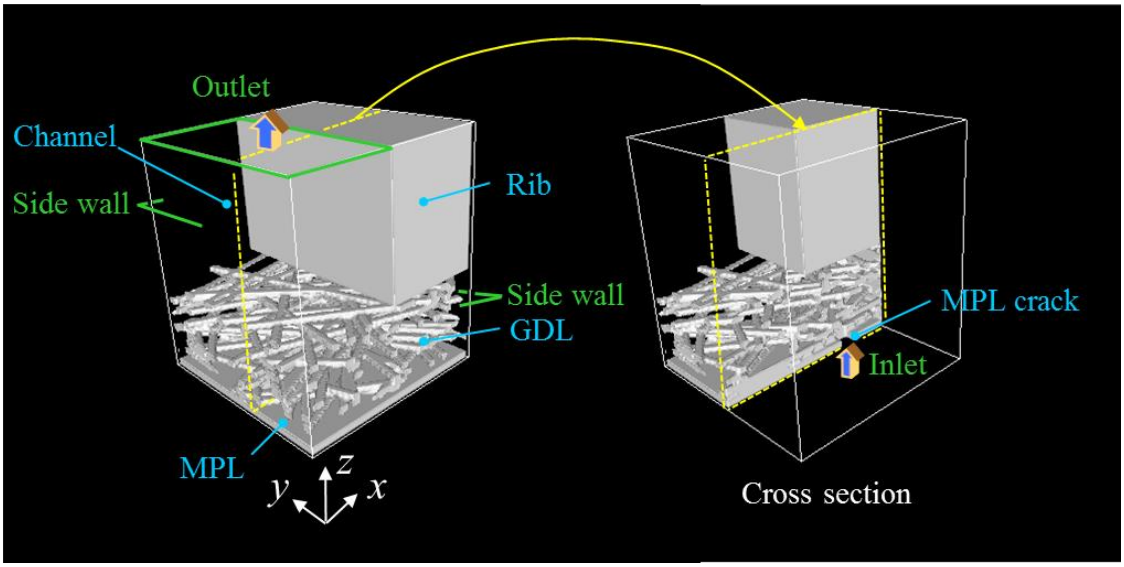

Figure 3.1 Simulation domain and simulation boundaries

3.2 Scale Model Experiment

Liquid water behavior in the GDL, the capillary number Ca = uμ/σ [3] is the governor force, while inertial and gravity forces are negligible in the complicated GDL structure due to very small pore diameter which is about 20-30 μ. The effect of viscous forces is also smaller than the capillary forces, as low flow velocity is present. In this case the velocity of water is u, μ represents the viscosity and σ indicates the interface tension. In an enlarge scale model, adjusting the capillary number would allow the water motion in the GDL to be similar. However, in the case of scale model, rather than the capillary force, gravitational and inertial forces become dominant. In order to neutralize the effects of gravitational and inertial forces, silicone oil (SHIN-ETSU, KF-56A) was used for water and water for air. When silicon oil is applied, the viscosity ratio becomes M = 16.7, whereas the real two-phase rate is around M = 17: here the viscosities of silicone oil and water are μ_{oil} = 1.49×10^{-2}Pa·s and μ_{water} = 8.90×10^{-4}Pa·s respectively. The densities of silicone oil and liquid water are ρ_{oil} = 995kg/m^3 and ρ_{water} = 997kg/m^3. This eliminates the gravitational effect. Moreover, the interfacial tension between silicon oil and water is σ = 2.56×10^{-2}N/m. A detailed discussion on the scale model experiment can be found in Reference 6.

Figure 3.2 (a) shows the picture of 240 times enlarged GDL model produced by the 3D printer. The 3D printer used in this study is is a ProJet®4500 (3D SYSREMS) with VisiJet C4 Spectrum. The resolution is 600×600 dpi and the layer thickness are 0.1 mm. Experimental setup for scale model experiment is showed Figure 3.3.

(a) Reproduced 240 times GDL model

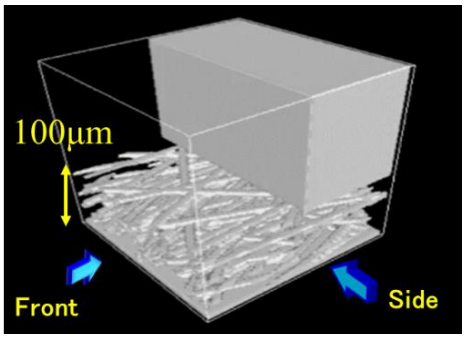

(b) LBM simulation domain

Figure 3.2 The picture on the left is 240 times enlarged scale model, the picture on the right LBM simulation domain of same model

The small differences between water and silicon oil's densities are accurately adjusted by controlling the temperature. The temperature controlled by a thermostatic chamber at 12°C in order to minimize buoyancy effects. The contact angle of the silicon measured by placing a droplet of silicon oil on a flat plate which is same material with scale model. The contact angle of silicon oil is 130°. As it can be seen from Figure 3.3, the scale model is installed in a water bath placed in the thermostatic chamber. The red silicon oil is injected in to the GDL from the hole at the bottom of the structure by a motor-driven syringe pump (YMC, YSP-201) at constant flow rate 2.18ml/s. This hole represents MPL crack. The fluid behaviour is recorded from the front and right sides through the acrylic walls by two CCD cameras which are also placed in the thermostatic chamber.

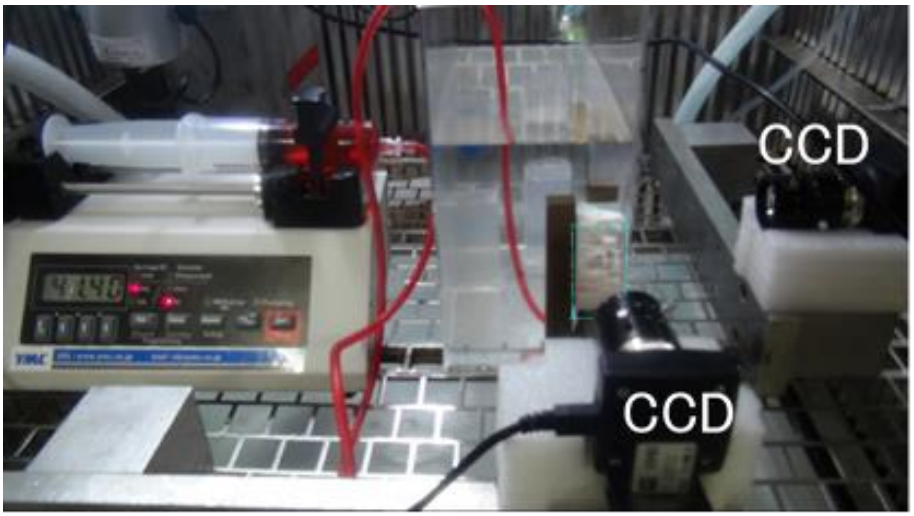

Figure 3.3 Experimental Setup

3.3 Effect of Hydrophilic Surface Treatment

In this study two identical enlarged model have been used to observe fluid flow inside of the GDL. Figure 3.4(a) is top view of the uniform GDL structure with 130° contact angle. Uniform GDL is enlarged model of commercially available GDL which wettability is same through whole structure. Figure 3.4(b) shows surface treated GDL which has similar structure with uniform GDL. However, it has been painted with an acrylic paint which gives 85° contact angle. In both case rib's wettability is determined as 60° contact angle.

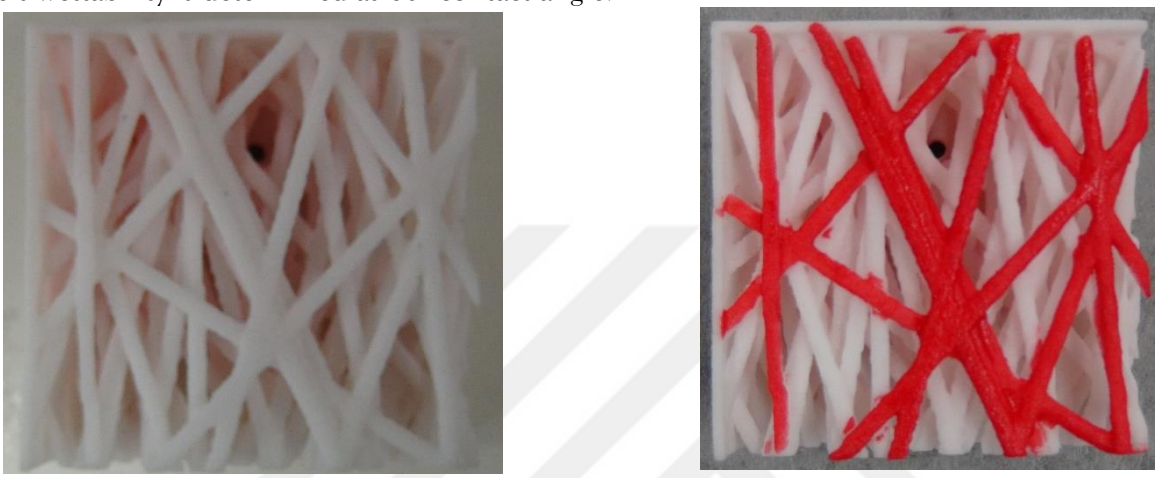

(a) Uniform GDL (b) Surface Treated GDL

Figure 3.4 Top view of structures

Furthermore, in order to simulate and compare water behaviour inside of the structure LBM simulation has been conducted. Figure 3.5(a) and Figure 3.5(b) shows uniform GDL structure domain and surface treated GDL domain in LBM simulation, respectively.

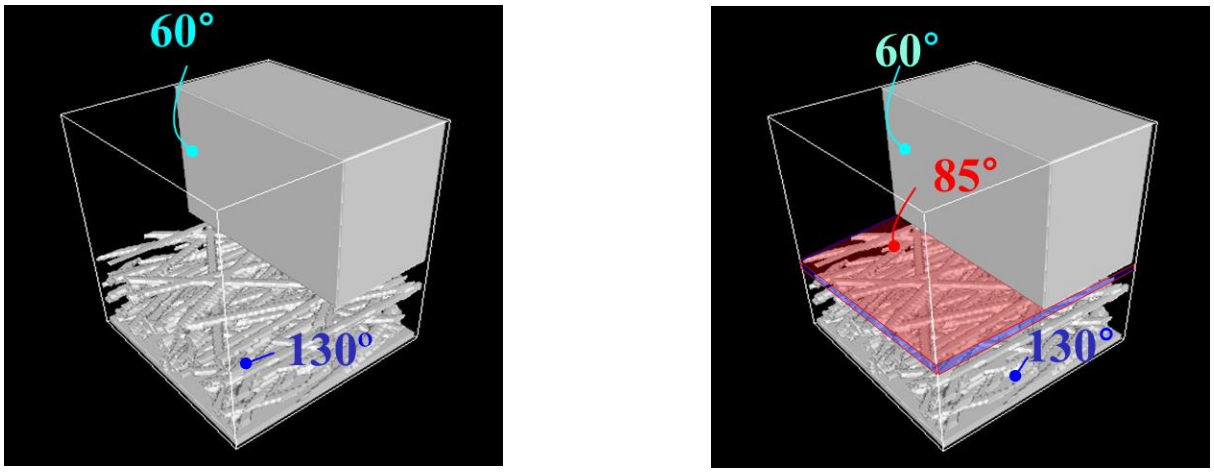

(a)Uniform GDL domain (b) Surface Treated GDL domain

Figure 3.5 The GDL structures in LBM domain

Firstly, uniform GDL structure has been simulated by LBM simulation. Figure 3.6 shows three steps of LBM simulation results. Figure 3.6 (a) shows initial stage of water movement in the

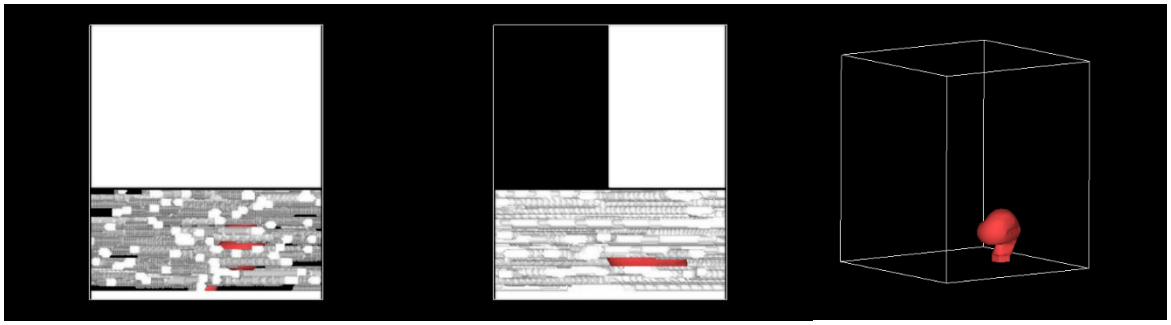

(a) t= 1.12 ms

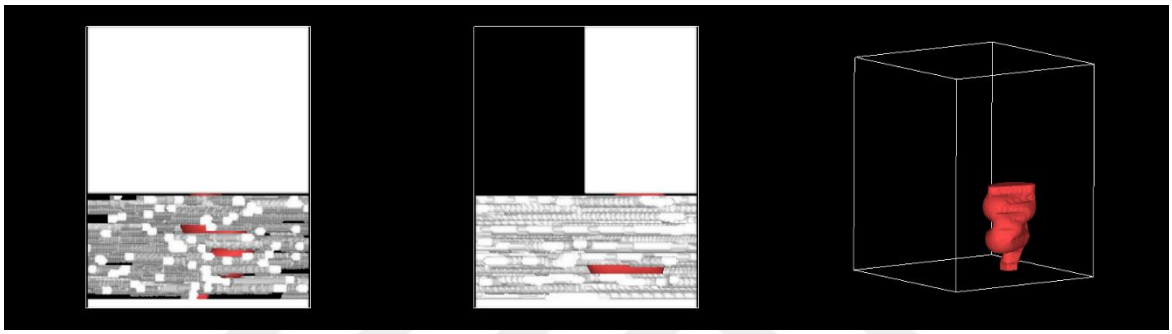

(b) t= 2.24 ms

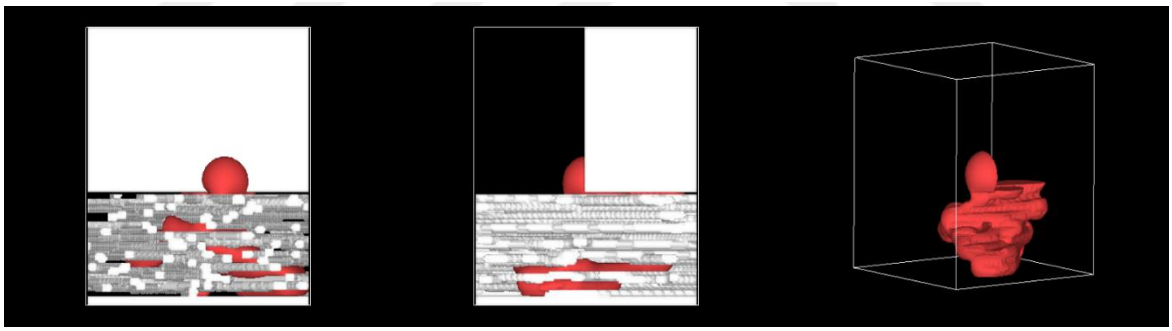

(c) t= 8.88ms

Figure 3.6 Simulation result of liquid water behavior in the uniform GDL

structure in 1.12 ms. In 2.24ms water has reached to the bottom of the rib (Figure 3.6 (b)). However, as it can be seen from Figure 3.6 (c) water is acumulated inside of the GDL until 8.8 ms which is the time water droplet emerges on the surface of the GDL.

Secondly, simulation of surface treated GDL with 85° contact angle has been conducted. Result of this simulation is shown in Figure 3.7. As it can be seen from Figures 3.7 (a) and (b) which show the initial stage and the timing when fluid reached the bottom of the rib, respectively, movement is totally same with uniform GDL simulation. However, Figure 3.7 (c) shows that

emerging of water droplet on the surface of the hydrophilic surface treated GDL is earlier than uniform GDL structure due to the hydrophilic surface treatment.

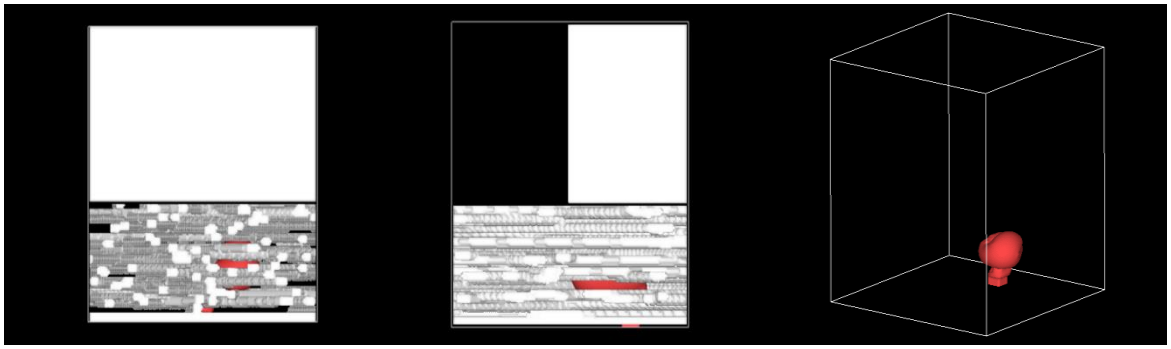

(a) t= 1.12 ms

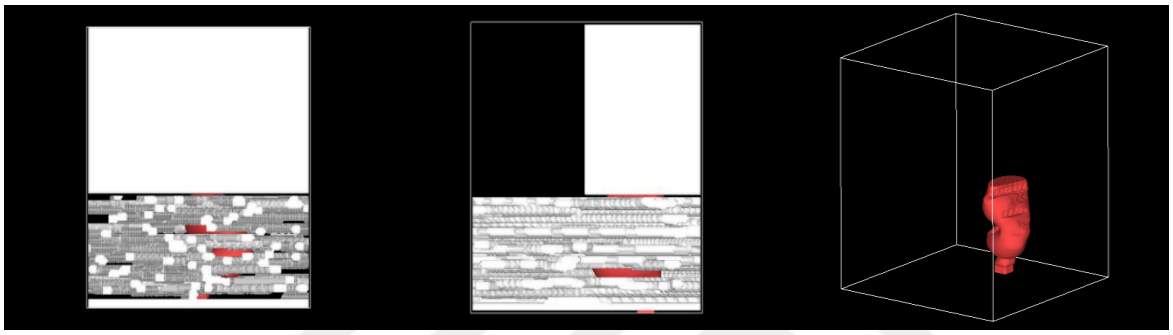

(b) t= 2.24 ms

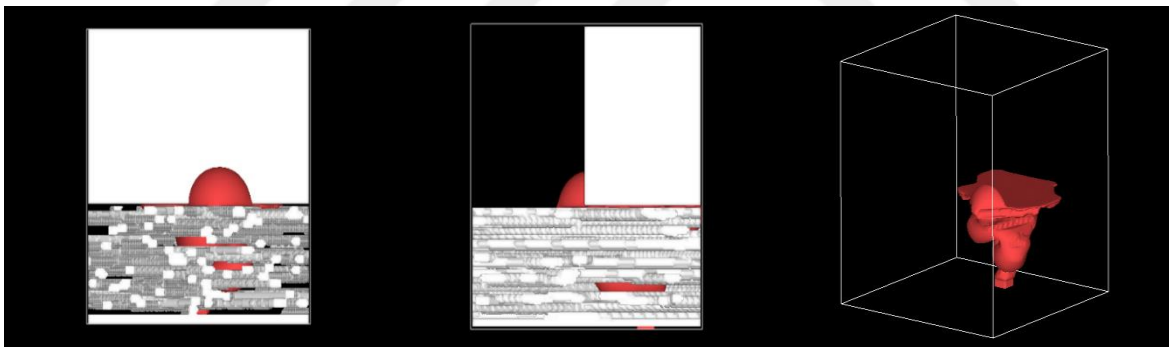

(c) t= 4.16 ms

Figure 3.7 Simulation result of liquid water behavior in 85° surface treated GDL

Thirdly, two above mentioned conditions have been applied to the 240 times enlarged scale model experiment. Figure 3.8 shows experimental results of uniform GDL. As it can be seen from the figure the liquid reached to the rib in 2 min. However, it takes 8 minutes for emerging on the surface of the GDL. From 2 minutes to 8 minutes the amount of liquid inside of the uniform GDL structure has increased.

(a) 1.0 min

(b) 2.0 min

(c) 7.0 min

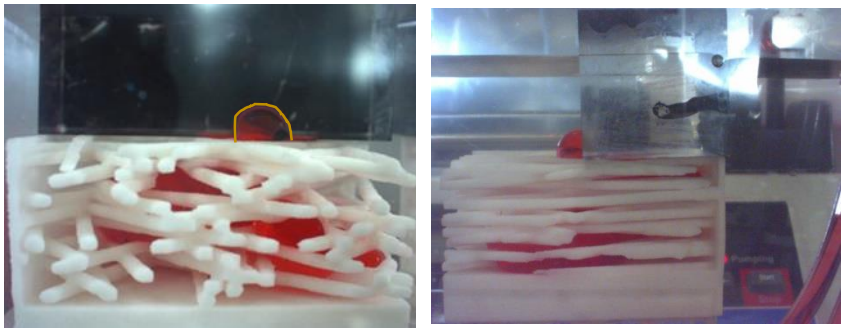

(d) 8.0 min

Figure 3.8 Experimental result of liquid behavior in uniform GDL

Furthermore, the result of hydrophilic surface treated GDL (Figure 3.9) shows that the fluid behavior inside of the structure is similar until 2 min which is the time liquid reached the rib. However, as it can be seen from Figure 3.9 (c), the liquid has emerged on the surface of the GDL without not much spreading in the structure in 5.2 minutes.

(a) 1.0 min

(b) 2.0 min

(c) 5.2 min

Figure 3.9 Experimental result of liquid behavior in hydrophilic surface treated GDL

The result of LBM simulations and scale model experiments shows that the excessive amount of water accumulate under the rib. This increases water content inside of the GDL structure which decrease fuel cell performance under high current density applications. However as it can be seen from Figures 3.7 and 3.9 hydrophilic surface treatment highly decreased amount

of water which accumulates under the rib.Thus, under the high current density operations hydrophilic surface treatment on hydrophobic GDL can improve fuel cell performance drastically.

4. EFFECT OF WETTABILITY DESIGN OF GDL ON PEFC PERFORMANCE

In this study three different wettability design has been applied on non-treated GDL with three different polytetrafluoroethylene (PTFE) content. Newly designed GDLs with different wettability patterns are employed in a single fuel cell. Detailed information about experimental setup can be found chapter 3. Furthermore, the performance of the GDLs has been compared by I-V curves.

4.1 Coating Process of GDL with Different Wettability Design

In this research ten per cent, twenty per cent and sixty per cent PTFE coating have been applied with dot and stripped designs on GDLs. Figure 4.1 shows the schematic diagram for dot design.

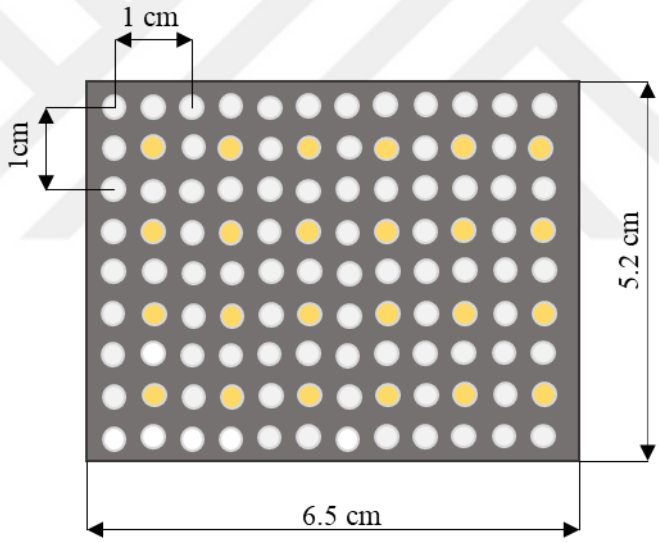

Figure 4.1 Schematic diagram of dot coating design

Yellow circles indicate the circle which is used for coating and diameter of each circle is three millimeters. Figure 4.2 shows 2mm-6mm stripped design on GDL. In this wettability design GDL has been coated stripped shape. Black colour shows coated columns. Width of the each black column is two millimetres and the length between two coated column is six millimetres. The size of the GDL same with dot shape designed GDL which witdt is 5.2 centimeters and length of the GDL is 6.5 centimeters. Furhermore, third design is 2mm-2mm stripped design on GDL. As it can be seen from Figure 4.3 black columns shows coated part of the GDL and width

of it is two milimeter. The distance between two coated coloum is two milimeters. The size of the GDL is the same with other two designs.

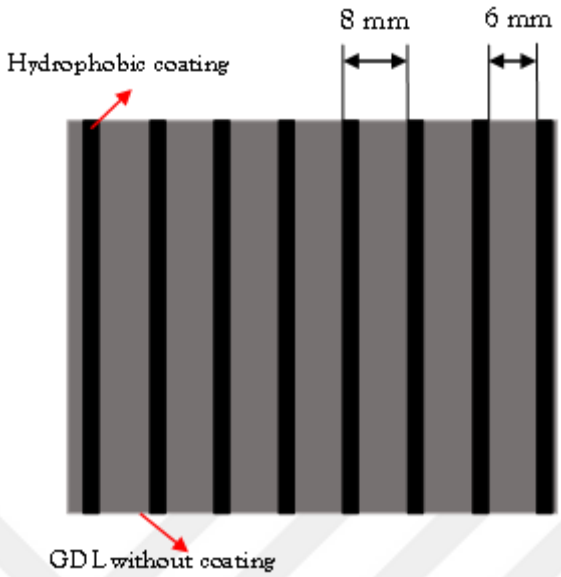

Figure 4.2 Schematic diagram of 2mm-6mm stripped design coating

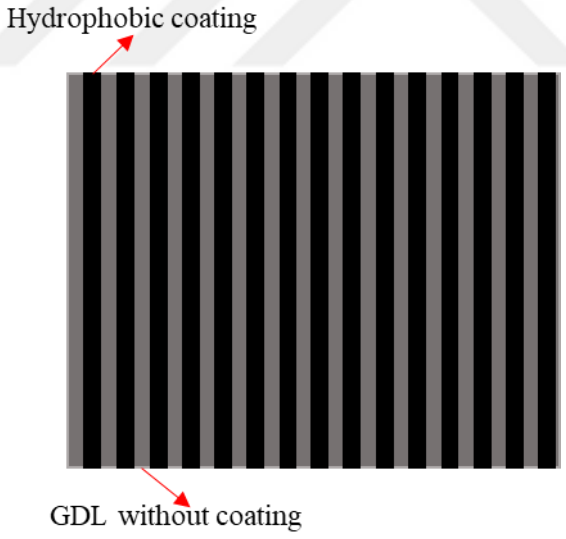

Figure 4.3 Schematic diagram of 2mm-2mm stripped design

In this study as a coating solution, Teflon PTFE DISP 30 from Chemours has been used. Solid content (%PTFE by weight) of the dispersion is sixty weight per cent and dispersion average particle size is 0.220 micrometer. To coat GDLs, three different solutions have been prepared. PTFE content in the prepared solutions are ten per cent, twenty percent and sixty per cent. In order to prepare ten and twenty percent coating solutions, H_2O has added proportionally to sixty

percent dispersion. In order to prepare solutions one-gram PTFE dispersion has been placed in a test tube and five-gram H_2O added for ten per cent solution and two-gram H_2O for twenty percent solutions. In order to make a homogeneous coating solution, prepared test tubes were mixed on MVM-10 vortex for ten minutes. The mixture was further sonicated for one hour. Mixing machines used for dilution process of PTFE can be seen from Figure 4.4.

Figure 4.4 Dilution process of PTFE

The frames that used to coat GDLs are shown in Figure 4.5. In order to coat GDL surface with a certain design, GDLs have cut 5.2 centimeters in width and 6.5 centimeters in length. Cut GDL has been placed on a glass palate. Prepared frame has been put on the GDL which placed on the glass plate. After placing the coating frame on the GDL, frame was tapped to the glass from its corners to ensure it would not move during coating process. To apply PTFE solution on GDL, a cotton swab has dipped in the solution for two second and applied on the surface of the GDL softly. After coating process has been completed, frame was removed on the glass plate and the newly coated GDL was placed in an oven at 90°C for one hour. After an hour, newly designed GDL has been put in a single cell to test its performance.

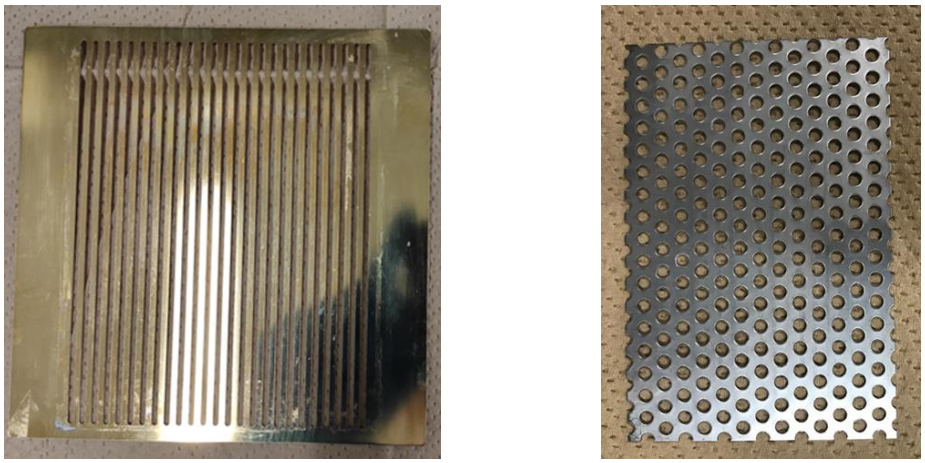

Figure 4.5 Frames used for coating

4.2 Result of the Newly Designed GDL with Wettability Pattern

In order to compare newly design GDLs, a GDL from SGL Group (Sigracet GDL 39AA) has been used as a reference. Reference GDL and newly designed GDLs are without MPL coating. Detailed information can be found from Reference 5. Wettability designed GDLs and reference GDL have been compared by I-V curves. Figure 4.6 shows the I-V curve of the reference GDL.

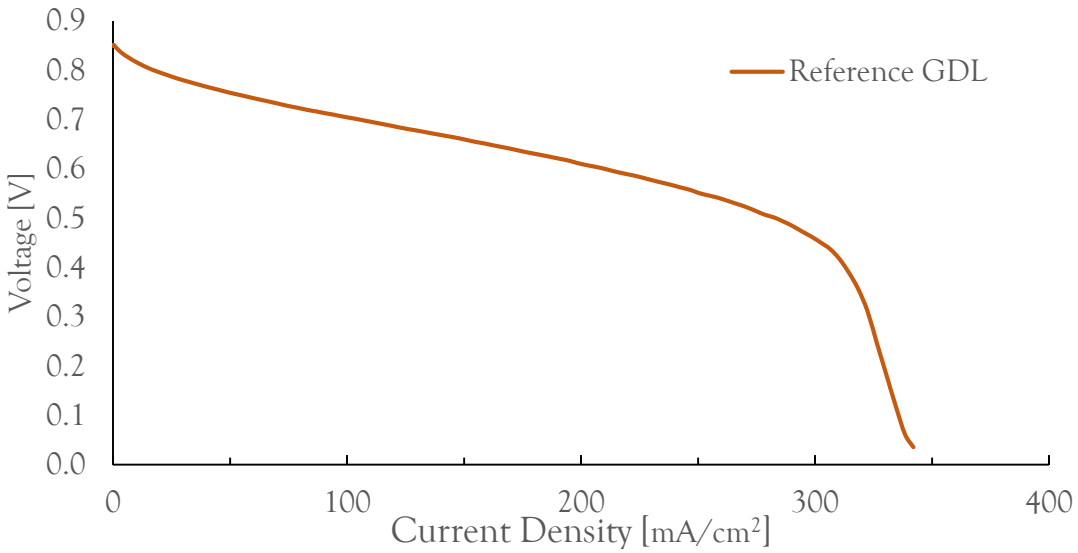

Figure 4.6 Reference GDL's I-V curve

As it can be seen from Figure 4.6 the limiting current density of reference GDL is around 340 mA/cm^2. Furthermore, Figure 4.7 shows experimental result of the 2mm-2mm stripped design with ten per cent, twenty per cent and sixty per cent PTFE solutions. As it can be seen from Figure 4.7 PTFE coating with ten per cent solution shows the best result. Moreover, the

graph shows that twenty per cent PTFE coated GDL shows better performance than reference GDL. However, sixty per cent PTFE coated GDL with 2mm-2mm stripped design performance lower than reference GDL.

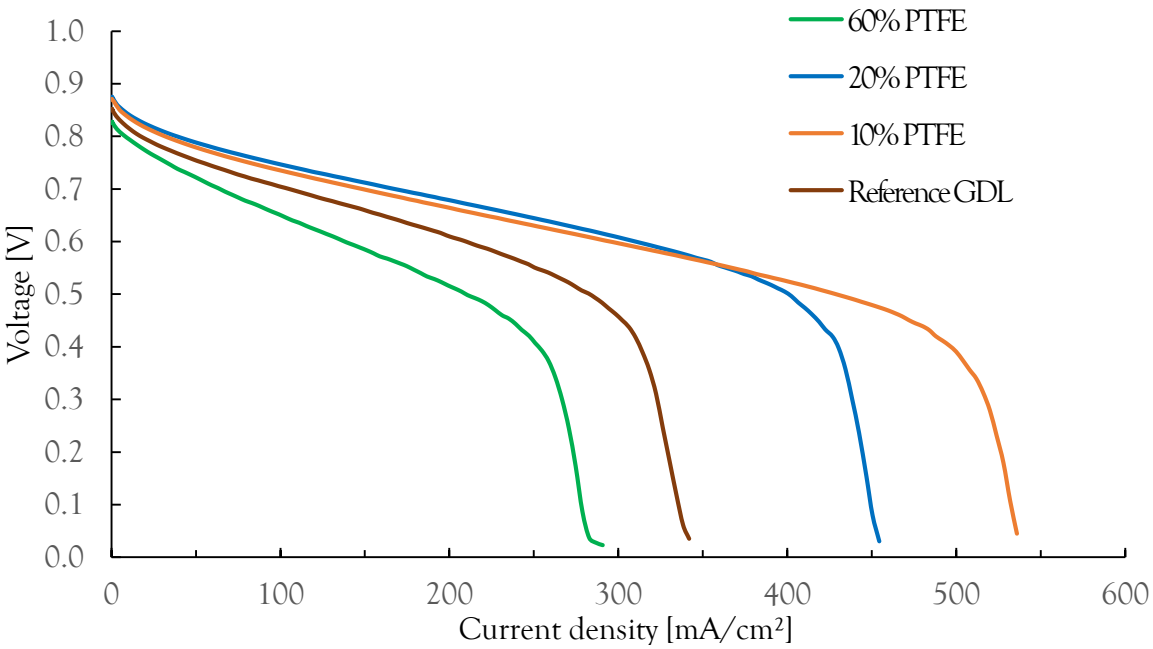

Figure 4.7 2mm-2mm stripped design coated GDL with different PTFE solutions

Due to the increase in hydrophobicity of the coated regions of the GDL, water accumulates inside of the non-coated part of GDL which is hydrophilic. Moreover, oxygen easily penetrates to the catalyst side using hydrophobic path inside of the GDL, which resultes in increases performance of ten per cent and twenty per cent coated GDL. However, when PTFE amount increases inside of the GDL, it starts to block pores of the GDL which resultes in water accumulation inside of the structure. Thus, sixty per cent PTFE coating shows lower performance than the reference GDL and ten per cent coating gives better performance than twenty per cent.

Figure 4.8 illustrates result of the dot designed GDL. As it can be seen from the graph ten per cent coated GDL's performance is better and limiting current density reached to 500mA/cm^2. Even though twenty per cent dot designed GDL's performance is better than reference GDL when compared to ten percent dot designed GDL it gives lower performance. This may be due to the decrease in pore size because of higher amount of PTFE content.

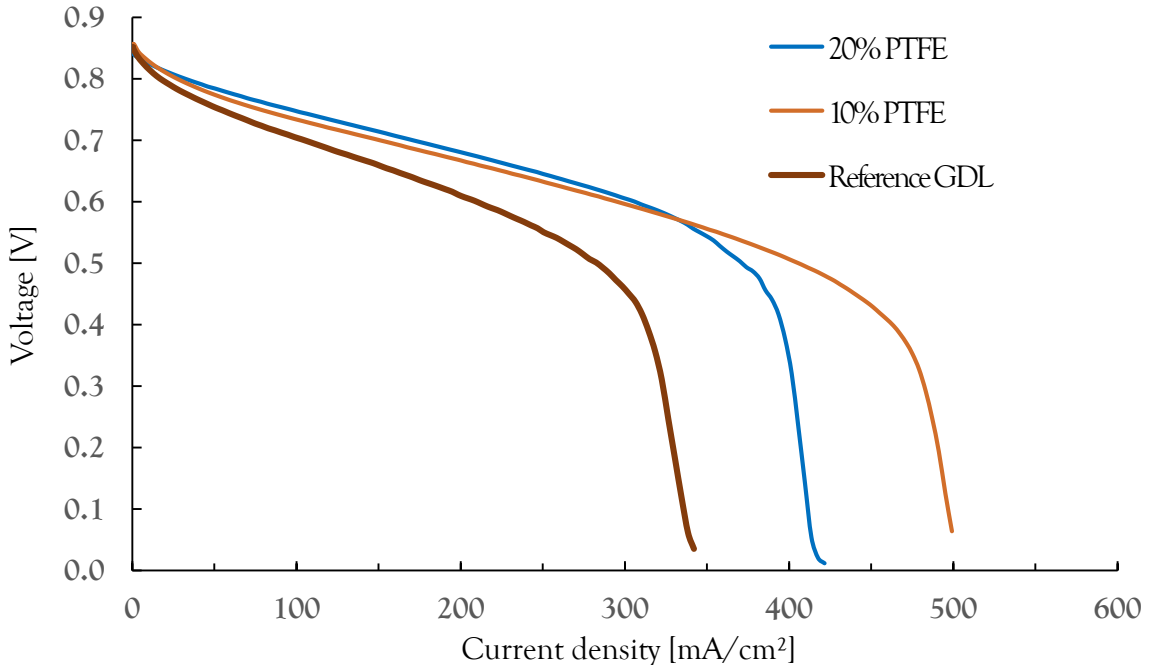

Figure 4.8 Performance of dot design coated GDL with different PTFE solutions

Figure 4.9 shows the result of 2mm-6mm stripped design coated GDL with different PTFE content. The results shows that ten per cent PTFE coating gives better result around 490 mA/cm^2. Twenty percent coating shows better performance than reference GDL, however it gives less performance than ten percent PTFE coated GDL.

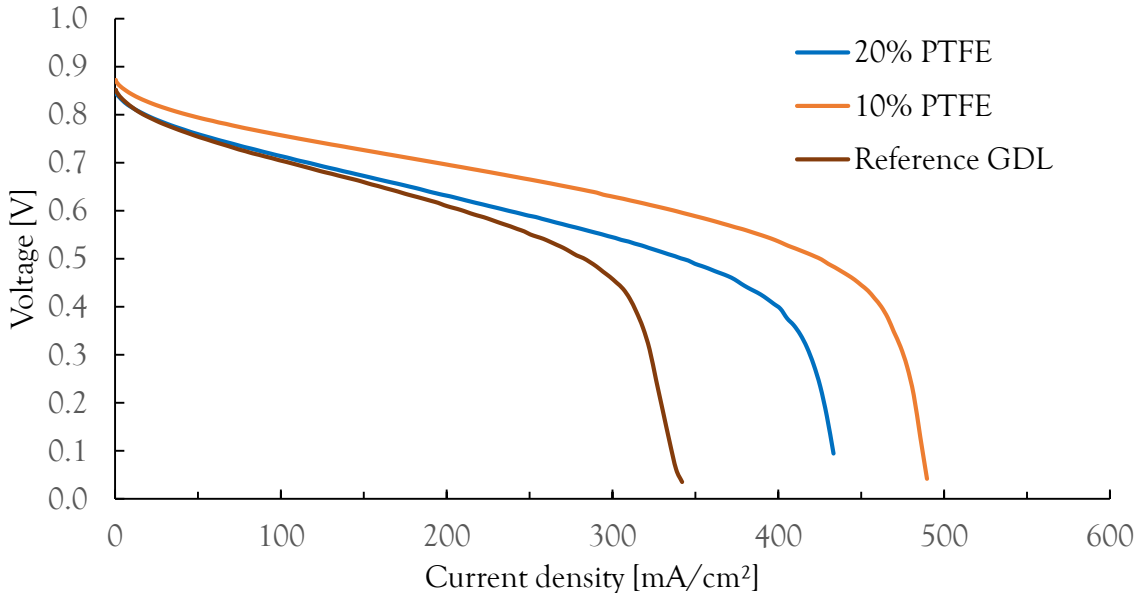

Figure 4.9 2mm-6mm stripped design coated GDL with different PTFE solutions

Coated GDL with different wettability designed can be seen from Figure 4.10

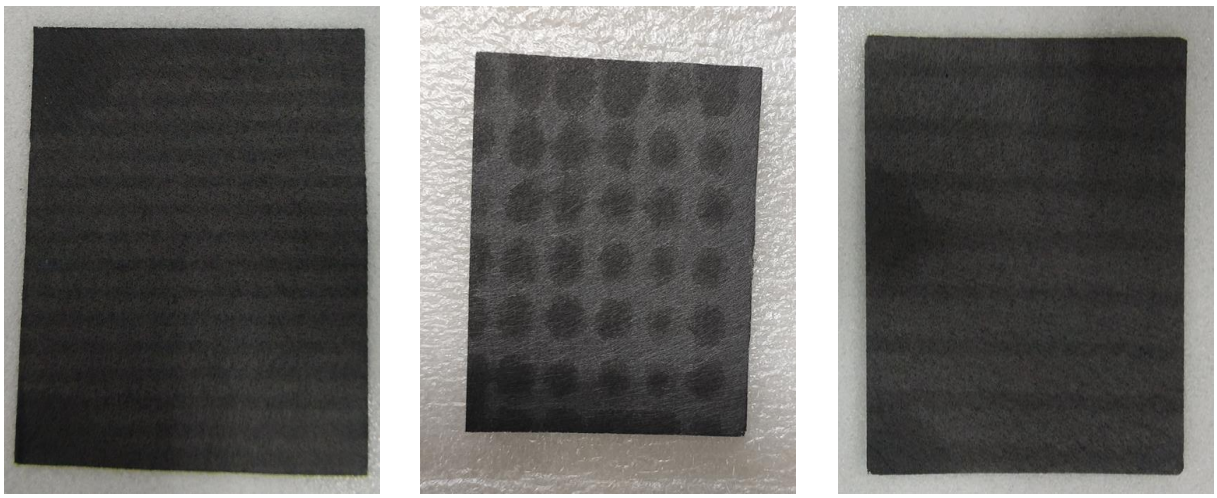

(a) (b) (c)

Figure 4.10 Various wettability designs of GDL

Figure 4.10 (a) is 2mm-2mm stripped design, dot designed is shown in Figure 4.10 (b) and 2mm-6mm striped design is in Figure 4.10 (c). As it is illustrated in Figure 4.10 the area between hydrophilic and hydrophobic part of a GDL is biggest in 2mm-2mm stripped designed GDL. Thus, the performance of the 2mm-2mm stripped design coated GDL is best in three designs. Figure 4.11 shows the comparison between different wettability designed GDL with coated ten per cent PTFE solution.

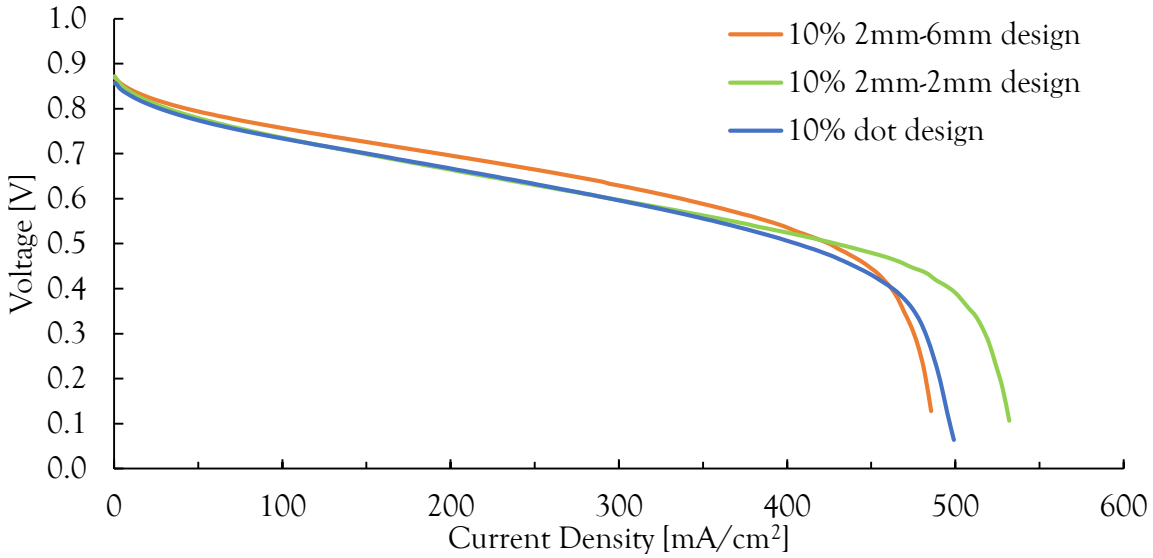

Figure 4.11 Comparison of different wettability design of ten per cent PTFE coating

As it can be seen from Figure 4.11 increase in the interaction area between hydrophilic and hydrophobic regions results in better cell performance. The interaction area between hydrophilic and hydrophobic regions can be describe as passage for water to move more hydrophilic regions. Thus, increase in the area between regions highly affects fuel cell performance. Because 2mm-2mm wettability design has larger interaction area between two regions, it gives better result than the other designs.

5. CONCLUSION

5.1 LBM Simulation and Scale Model Experiment

- LBM simulation has been conducted with uniform wettability GDL structure. It has been observed that water accumulate under the rib due to the high threshold pressure (capillary pressure) between GDL and its surface.
- Water behavior inside of the hydrophilic surface treated GDL with 85° contact angle has been simulated by LBM simulation. Results shows that due to the hydrophilic surface treatment on hydrophobic GDL water content inside of the GDL structure which accumulate under the rib decreased dramatically.
- 240 times enlarged scale model experiments have been conducted.
- Scale model experiments results are similar with LBM simulation's results. This shows that adjusting capillary numbers and viscosity ratio of two immiscible liquids, it is possible to observe similar fluid behavior inside of the scale model. However, it is important to eliminate bouncy effect and gravitational forces.

5.2 Effect of Wettability Design of GDL on PEFC Performance

- Three different wettability designs which are 2mm-2mm, 2mm-6mm and dot designed with three different PTFE solutions which are 10 per cent, 20 per cent, and 60 per cent GDL have been tested.
- The single fuel cell test's results show that 2mm-2mm designed GDL gives better result for three different PTFE loading.
- The results indicate that when the area between hydrophilic and hydrophobic regions increase, fuel cell performance increases dramatically.
- When the result of different PTFE loading compared, it shows that after a certain amount of loading, PTFE particles start to block GDL pores which gives poor performance.
- This study shows that using different wettability patterns it is possible to create dedicated path ways for oxygen and water transportation in GDL in order to increase performance of PEFCs under the high current density operations.

REFERENCES

[1] International Energy Agency, 2018, Electricity statistic,

[https://www.iea.org/]

[2] Ecotricity,2018, When will fosil fuels run out?,

[https://www.ecotricity.co.uk/our-green-energy/energy-independence/the-end-of-fossil-fuels]

[3] U. Pasaogullari, C.Y.Wang, 2004, J. Electrochem. Soc.151 A399–A406.

[4] Larminie J., Dicks A., 2003, *Fuel Cell Systems Explained*, J. Wiley, pp 1-24.

[5] SGL Carbon, Sigracet Fuel Cell Component,

[https://www.sglcarbon.com/en/markets-solutions/material/sigracet-fuel-cell-components/]

[6] Sakaida S., Tabe Y. and Chikahisa T., 2017, Large scale simulation of liquid water transport in a gas diffusion layer of polymer electrolyte membrane fuel cells using the lattice Boltzmann method, Journal of Power Sources, Vol.361 pp.133–143.

[7] Inamuro T., Tomita R. and Ogino F., 2003, Lattice Boltzmann simulations of drop deformation and breakup in shear flows, International Journal of Modern Physics B, Vol.17, pp.21–26.

[8] Fuel Cell Store, Teflon™ PTFE DISP 30 Fluoropolymer Dispersion, [https://www.fuelcellstore.com/fuel-cell-components/dispersions/teflon-dispersions/teflon-disp30]

[9] Sehkyu Park, Jong-Won Lee, Branko N. Popov, 2012, A review of gas diffusion layer in PEM fuel cells: Materials and designs, International Journal of Hydrogen Energy, 375850-5865.